Transactions, SMiRT-22
San Francisco, California, USA - August 18-23, 2013
Division IX (include assigned division number from I to X)

SEISMIC PERFORMANCE OF LOW ASPECT RATIO REINFORCED CONCRETE SHEAR WALLS

Bismarck N. Luna[1], Jonathan P. Rivera[1], Joshua F. Rocks[2], Caglar Goksu[3] and Andrew S. Whittaker[4]

[1] PhD Candidate, Department of Civil, Structural and Environmental Engineering, University at Buffalo, Buffalo, NY
[2] Associate Engineer, Constellation Energy Nuclear Group, LLC, Lycoming, NY
[3] Postdoctoral Researcher, Civil Engineering Department, Istanbul Technical University, Istanbul, Turkey
[4] Professor and Chair, Department of Civil, Structural and Environmental Engineering; Director, MCEER; University at Buffalo, Buffalo, NY

ABSTRACT

Although low aspect ratio shear walls are widely used in safety-related nuclear structures, their hysteretic behavior, including peak strength and effective elastic stiffness, has not been adequately characterized to enable robust performance and risk assessment. The US National Science Foundation funded a Network for Earthquake Engineering Simulation (NEES) research project on shear walls of conventional and composite construction to better understand the seismic behavior of these widely used structural elements. A total of 16 rectangular, low aspect ratio concrete shear walls (12 conventionally reinforced concrete and four composite) were built and tested at the University at Buffalo (UB). This paper addresses the response of the conventionally reinforced shear walls.

The test data confirmed that design equations in codes and standards are unable to predict peak shear strength and that the scatter in the predictions is significant. The hysteretic response of the test specimens degraded quickly at cycles to displacement greater than that associated with peak strength, questioning the behavior of nuclear structures that incorporate shear walls for earthquake shaking more intense than design basis. The effective stiffness of the test specimens were substantially lower than those calculated using the predictive equations of ASCE 43-05 and ASCE 41-06, which is problematic for dynamic analysis, generation of in-structure floor response spectra, and risk assessment.

INTRODUCTION

Low aspect ratio structural walls (ratio of height to length of two or less) are widely used in safety-related nuclear structures to resist lateral loadings and provide containment or confinement. Recent studies by the authors and others [Gulec et al. (2008), Gulec and Whittaker (2009), Gulec et al. (2010), Gulec and Whittaker (2011)] have clearly demonstrated that the seismic performance of conventional low aspect ratio walls cannot be accurately estimated using existing predictive equations or hysteretic models. Although building codes and standards of practice provide equations to predict the maximum shear resistance of a reinforced concrete shear wall, the equations provide biased estimates of peak shear strength and the predictions are scattered (Gulec and Whittaker, 2011). Accurate prediction of the cyclic response of walls is important for both code-based design and seismic performance assessment.

To improve the understanding of the cyclic response of low aspect ratio walls, the US National Science Foundation (NSF) funded a Network for Earthquake Engineering Simulation (NEES) research project on shear walls of conventional and composite construction. Sixteen rectangular, low aspect ratio concrete shear walls were built and tested at the NEES facility at the University at Buffalo (UB): 12 conventionally reinforced walls and four steel-concrete (SC) walls. Two additional reinforced concrete shear walls were tested using hybrid simulation at the University of California, Berkeley.

This paper addresses the response of the 12 conventionally reinforced (RC) shear walls tested at UB. Information on the four SC walls is reported elsewhere at this conference (Epackachi et al., 2013). Whyte and Stojadinovic (2012) report the results of the hybrid simulation tests.

EXPERIMENTAL PROGRAM

Twelve large-size, low aspect ratio, rectangular, RC shear wall specimens (denoted SW1 to SW12) were built and tested at the NEES facility at UB. The length and thickness of the test specimens were 10 feet and eight inches, respectively. The design variables considered in developing the portfolio of test specimens included wall aspect ratio (h_w/l_w), day-of-test concrete compressive strength ($f_c^{'}$), vertical and horizontal reinforcement ratio (ρ_l, ρ_t), yield and ultimate strengths of the reinforcements (f_y, f_u), splices in vertical reinforcement, and boundary elements. The properties of the walls are summarized in Table 1. The test program was executed in two phases: Phase I (SW1-SW7) and Phase II (SW8-SW12). The Phase II walls were designed after preliminary analysis of the test data from the Phase I walls. Pre-construction analysis of the walls indicated that SW1 would fail due to both flexure and shear, and that SW2 through SW12 would fail in shear.

Table 1: Properties of the test specimens.

Wall	h_w/l_w	Web		Boundary element		Mechanical splices	$f_c^{'}$ (ksi)	f_y (ksi)	f_u (ksi)
		ρ_l (%)	ρ_t (%)	ρ_l (%)	ρ_t (%)				
SW1	0.94	0.67	0.67	-	-	-	3.6	67	102
SW2	0.54	1.0	1.0	-	-	yes	7.0	63	87
SW3		0.67	0.67	-	-	yes	7.8	63	87
SW4		0.33	0.33	-	-	-	4.2	67	102
SW5	0.33	1.0	1.0	-	-	-	4.3	67	102
SW6		0.67	0.67	-	-	-	3.8	67	102
SW7		0.33	0.33	-	-	-	3.8	67	102
SW8	0.54	1.5	1.5	-	-	-	3.5	67	102
SW9		1.5	0.67	-	-	-	4.3	67	102
SW10		1.5	0.33	-	-	-	4.6	67	102
SW11		0.67	0.67	1.5	1.5	-	5.0	67	102
SW12		0.33	0.33	2.0	2.0	-	5.0	67	102

The foundation of each shear wall was post tensioned to the strong floor in the laboratory using 14, 1.5 inch diameter Dywidag bars. Lateral loads were applied to the walls using two high force-capacity actuators that were horizontally inclined by 9 degrees with respect to the longitudinal axis of the walls. The actuators imposed displacements on the shear walls via custom-made brackets and thick steel plates that were post tensioned to either side of the specimen. Incremental cyclic displacements were imposed on the walls to indirectly simulate the effects of earthquake shaking. Displacement transducers in the actuators were used to control the lateral displacement of the walls. (Errors are inevitable with this control strategy at very small values of lateral displacement because of nonlinear slip and movement within the actuator clevis.) Load cells in the actuators measured the applied load. Figure 1 is a photograph of SW2 prior to testing.

No axial load was applied to the specimens because a) the axial stresses in low aspect ratio walls are typically small, and b) the challenges involved with imposing even low axial loads on walls with an

area of 1,000 square inches and maintaining a constant axial load at relatively large lateral displacements are difficult to overcome.

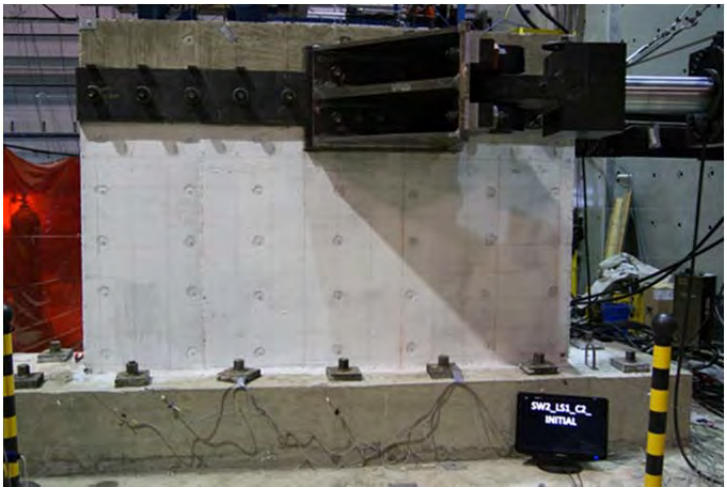

Figure 1. Specimen SW2 setup

INSTRUMENTATION

Traditional displacement transducers were used to measure the in-plane and out-of-plane displacements of each wall. The Krypton K600 Optical Measurement System (Nikon, 2013) was used to monitor displacements across one face of each wall, using LED sensors installed on a rectangular grid. Data from this dense grid of sensors enabled calculation of the contributions of flexure, shear and base slip to the total lateral displacement. Traditional transducers and LED sensors were installed to monitor lateral displacement and rotation of the foundation as a function of applied lateral load.

A rectangular grid was marked on the opposite face of the wall to the LED sensors to help monitor cracks and to facilitate interpretation of GigaPan (GigaPan, 2013) images of the cracked wall. Strain gages capable of measuring 15% strain were installed on the horizontal and vertical reinforcement in each wall. An average of 52 and 84 strain gages were installed on Phase I and Phase II walls, respectively. Figure 2 is a photograph of SW8 after instrumentation showing the grid of LED sensors.

GLOBAL RESPONSE

Figure 3 presents the measured force-displacement relationships for walls SW8, SW9 and SW10. The values inside the parenthesis in the title of each figure correspond to (1) aspect ratio, (2) horizontal reinforcement ratio, (3) vertical reinforcement ratio and (4) concrete compressive strength. The force was calculated using load cells in the actuators. The lateral displacement was calculated from in-plane string potentiometers attached at the centerline of loading. (The lateral displacement and rotation of the foundation, as measured by the Krypton system and string potentiometers, were negligible.) The three walls have an aspect ratio of 0.54 and a vertical reinforcement ratio of 1.5%. Some of the key observations from these figures are:

- The hysteretic response of SW8 and SW9 are qualitatively similar, measured here in terms of peak strength and loss of stiffness and strength with repeated cycling beyond the displacement corresponding to peak strength. The *pinching* of the hysteresis loops is attributed to sliding at the base, which occurs after the peak strength is attained.
- The peak shear strengths of SW8 and SW9 are similar, although SW9 has much less horizontal reinforcement, which suggests that above a threshold value, the effect of the horizontal reinforcement ratio on peak strength is small.

- The drift capacity is substantially affected by the horizontal reinforcement ratio.
- The rate of loss of shear strength is affected by the horizontal reinforcement ratio, below a threshold value.

Figure 2. Specimen SW8 instrumentation

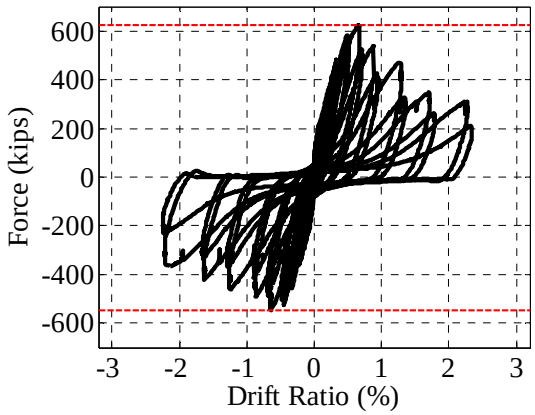

a. SW8 (0.54, 1.5%, 1.5%, 3500 psi)

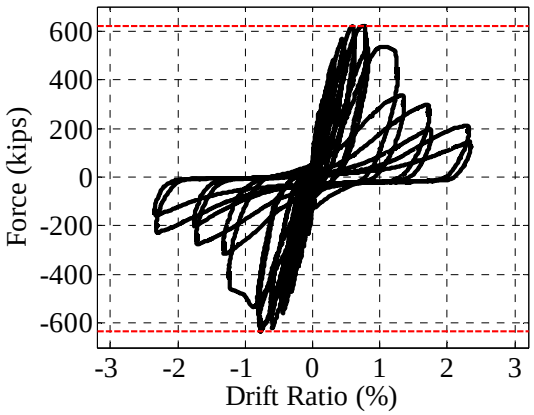

b. SW9 (0.54, 0.67%, 1.5%, 4300 psi)

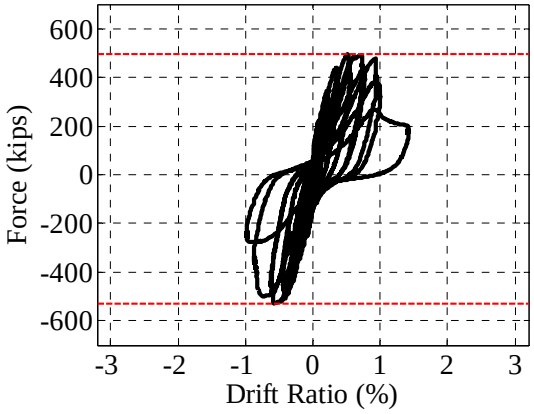

c. SW10 (0.54, 0.33%, 1.5%, 4600 psi)

Figure 3. Global force-displacement relationships of SW8, SW9 and SW10.

Photographs of the damage on walls SW9 and SW10 are presented in Figure 4 at drifts of approximately 1.2% (SW9) and 1.4% (SW10). The red arrows identify the direction of loading at the instant the photograph was taken. Although the drift ratios are similar, the performance of the two walls is very different: SW10 has failed in diagonal tension whereas moderate crushing of concrete is observed in SW9. The inclined cracks in SW9 are narrow and closely spaced, and this wall may provide confinement and/or containment at a drift ratio of 1.2%. The wide inclined crack in SW10 at a drift ratio of 1.4% dominates the behavior of this wall, which provides neither confinement nor containment.

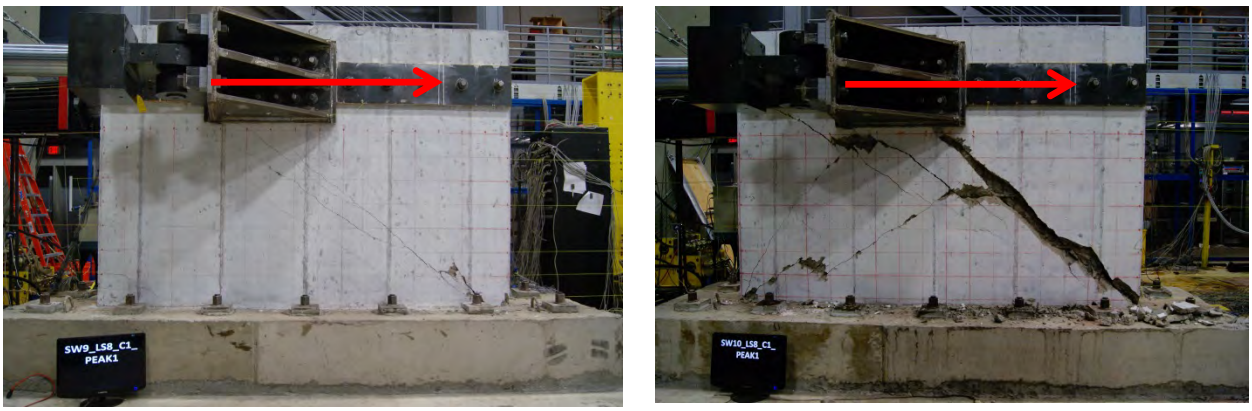

a. SW9 (Drift ratio = 1.2%) b. SW10 (Drift ratio = 1.4%)

Figure 4. Photos of the damage on SW9 and SW10.

The peak forces and the corresponding drift ratios (lateral displacement at the centerline of loading divided by the distance between the centerline of loading and the top of the foundation) for the 12 walls are reported in Table 2. Importantly, many of the walls achieve their peak resistance at drift ratios greater than 1%, which is counterintuitive, especially for the shear-critical walls (SW2 to SW12).

Table 2: Peak shear strength and corresponding drift ratio.

Wall	SW											
	1	2	3	4	5	6	7	8	9	10	11	12
Peak shear strength (kips)	253	563	468	226	726	570	318	623	633	528	424	416
Drift ratio (%)	1.3	1.3	2.1	1.1	0.9	0.8	0.4	0.7	0.8	0.6	0.6	1.2

SHEAR STRENGTH

Equations are provided in building codes and standards of practice to predict the peak shear strength of RC walls. Each equation uses design variables such as compressive strength of concrete, yield strength of reinforcement, reinforcement ratio and aspect ratio. The nominal shear strength of the 12 walls calculated using equations from chapters 11 and 21 of ACI 318-11 (2011), Barda et al. (1977), Wood (1990) and Gulec and Whittaker (2011) are presented together with the measured peak shear strength in Figure 5. (The measured peak strength is the average of the peak strengths in the first and third quadrants.) It is evident from the figure that a) there is a significant scatter in the predictions of peak shear strength, b) none of the equations are suitable for either design or performance assessment in their current form, and c) the variables used in the predictive equations are incomplete.

The Barda equation produces unconservative predictions for the rectangular walls, with over-predictions by more than a factor of two in three of the walls. The empirical equation derived by Gulec and Whittaker provides conservative (but biased) estimates of peak shear strength but predicted reasonably well the strengths of walls SW1, SW4, SW7 and SW10.

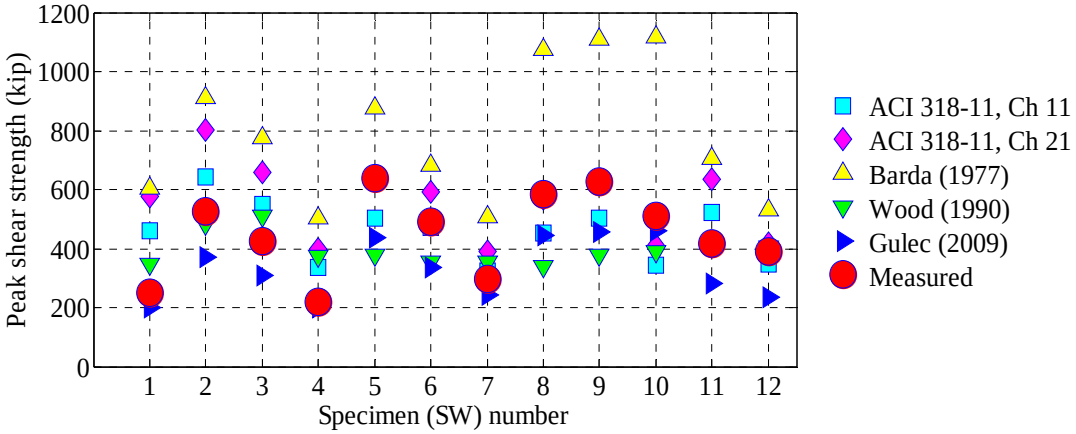

Figure 5. Measured and predicted peak shear strength.

LATERAL STIFFNESS

Values of effective stiffness for shear walls are needed for both design and performance (risk) assessment of safety-related nuclear structures. ASCE 43-05 (2005) and ASCE 41-06 (2006) provide guidance on the effective stiffness of structural components, where the values are assumed to be appropriate for loadings up to the peak resistance. For analysis and design of nuclear power plants, essentially *elastic* response is assumed for design basis shaking, and so the chosen value of effective stiffness impacts the seismic forces used for design of the primary structure and the in-structure floor spectra used for the design of safety-related secondary systems.

Figure 6 presents the generic load-deformation relationship specified in ASCE 41-06. Point B represents the yield point, point C represents the nominal strength and point D represents the loss of significant strength to a residual value. For walls whose response is dominated by shear, the strength associated with points B and C are taken to be the same. To calculate effective stiffness (the slope of line AB), ASCE 43-05 recommends the use of 100% of the shear and flexural rigidities whereas ASCE 41-06 recommends the use of 80% of the flexural rigidity and 100% of the shear rigidity for uncracked walls. For cracked walls, ASCE 43-05 recommends a 50% reduction in both shear and flexural rigidities and ASCE 41-06 recommends a reduction of 50% in flexural rigidity and no reduction in shear rigidity. Table 3 presents data on the lateral stiffness of the 12 walls. Day-of-test concrete compressive strength, equation 8.5.1 of ACI 318-11 for Young's modulus and Poisson's ratio equal to 0.2 were used in the calculations. The initial stiffness was calculated from the first load step in each test, which involved force less than 20% of peak strength and a drift ratio less than 0.04%. The secant stiffness was calculated at the point of peak shear strength. The calculated initial stiffness ranges between 20% and 50% of the effective stiffness recommended by ASCE 43-05 for uncracked wall sections. The secant stiffness at peak resistance is as low as 3% of the effective stiffness recommended by ASCE 43-05 for cracked wall sections. A gross over-prediction of wall stiffness may lead to an under-prediction of seismic demands for nuclear structures on rock sites and inappropriate floor response spectra for the seismic qualification of secondary systems.

The reason why the walls are much more flexible than predicted using guidance in codes and standards is not yet known. Sozen and Moehle (1993) observed that measured initial stiffness was less than the calculated theoretical initial stiffness and opined that the difference was due to 1) the cracks

invisible to the eye present before the test, and 2) deformability of the base girder. No foundation (base girder) rotation was observed in the twelve tests reported above. The presence of micro-cracks in the concrete near the base of the wall, due to restrained shrinkage associated with the large foundation and the reinforcement, may be the cause. The effect of restrained shrinkage on the stiffness of shear walls has been reported by Palermo and Vecchio (2002) and is being investigated by the authors using the test data and numerical simulations.

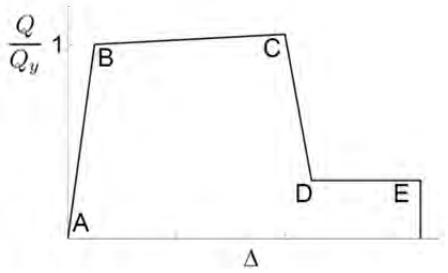

Figure 6. ASCE 41-06 force-deformation relationship (ASCE 41-06, 2006)

Table 3: Lateral stiffness of the wall specimens.

Wall	Theoretical / ASCE 43-05 *uncracked* (C2) kips/in	Calculated initial (C3) kips/in	$\frac{C_3}{C_2}$	ASCE 43-05 *cracked* (C5) kips/in	Secant stiffness at peak strength (C6) kips/in	$\frac{C_6}{C_5}$
SW1	4890	1840	0.38	2445	300	0.12
SW2	19710	4200	0.21	9855	690	0.07
SW3	20810	10170	0.49	10405	340	0.03
SW4	15270	2850	0.19	7635	320	0.04
SW5	30530	8900	0.29	15265	1250	0.08
SW6	28700	7570	0.26	14350	1090	0.08
SW7	28700	12260	0.43	14350	1090	0.08
SW8	13940	5370	0.39	6970	1380	0.20
SW9	15450	4980	0.32	7725	1250	0.16
SW10	15980	5250	0.33	7990	1400	0.18
SW11	16660	4090	0.25	8330	1170	0.14
SW12	16660	3850	0.23	8330	520	0.06

STRENGTH DEGRADATION

Walls in buildings and safety related nuclear structures are expected to sustain their strength for multiple cycles of loading at and beyond the displacement corresponding to peak shear strength. This sustained strength is represented by the yield plateau (line BC) in the ASCE 41-06 force-deformation curve of Figure 6.

Gulec et al. (2008) assembled a database of 120 rectangular walls and quantified the loss of strength with repeated cycling after the walls had achieved the peak strength. According to Gulec et al. (2008), the greatest percentage of loss of strength is observed in those walls with aspect ratios of less than 1.0. Figure 7 shows the loss of strength in SW1 with repeated cycling to displacements equal to or greater than that at peak strength. The values enclosed in parenthesis in the title of Figure 7 are identical to that of Figure 3. To quantify the loss of strength in the twelve walls, shear strengths V_{peak}, V_{peak2}, V_{peak3} and V_{peak4} (marked with red circles in Figure 7) were extracted from the first quadrant hysteresis loops of each

specimen. (V_{peak} corresponds to the peak shear strength at a displacement Δ_{peak}; V_{peak2} corresponds to the shear strength at the second excursion to the displacement Δ_{peak}, and so on for subscripts 3 and 4.) Table 4 presents the ratios V_{peak2}/ V_{peak}, V_{peak3}/ V_{peak} and V_{peak4}/ V_{peak}. On the second (third) excursion to Δ_{peak}, the shear strength is as low as 60% (40%) of the peak shear strength. Although the walls are expected to sustain the peak strength at multiple cycles of loading, it is evident from the ratios presented in Table 4 that the 12 walls tested show a rapid loss of strength after achieving their peak shear strength. This loss of strength (and stiffness) should be addressed for design basis and beyond design basis calculations.

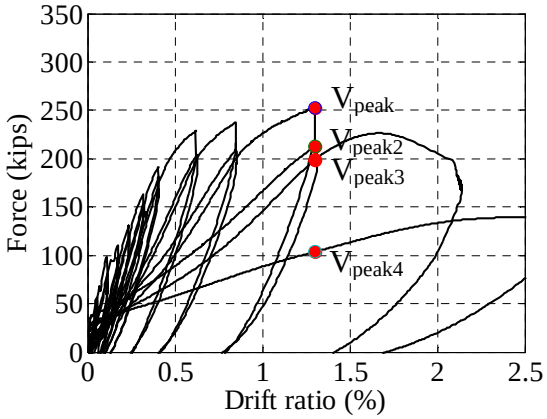

Figure 7. First quadrant hysteresis loops of SW1 (0.94, 0.67%, 0.67%, 3600 psi)

Table 4: Strength degradation.

Wall	$\frac{V_{peak2}}{V_{peak}}$	$\frac{V_{peak3}}{V_{peak}}$	$\frac{V_{peak4}}{V_{peak}}$
SW1	0.84	0.79	0.41
SW2	0.79	0.70	-
SW3	0.60	0.42	0.13
SW4	0.72	0.67	0.33
SW5	0.92	0.40	-
SW6	0.86	0.79	0.34
SW7	0.84	0.75	0.46
SW8	0.80	0.68	0.45
SW9	0.86	0.80	0.33
SW10	0.92	0.90	0.47
SW11	0.82	0.75	0.52
SW12	0.77	0.73	0.44

CONCLUSION

Twelve large-size, low aspect ratio, rectangular, reinforced concrete shear walls were built and tested at the University at Buffalo. The key findings of this study are:

1. There is a significant scatter in the shear strength of the 12 walls predicted using equations from chapters 11 and 21 of ACI 318-11 (2011), Barda et al. (1977) and Wood (1990): confirming the prior observation of Gulec et al. (2008). The empirical equation derived by Gulec and Whittaker provides

conservative (but biased) estimates of peak shear strength with reasonably good predictions for four of the 12 walls.

2. The initial stiffness of the 12 walls was substantially lower than the effective stiffness recommended by ASCE 43-05 (2005) and ASCE 41-06 (2006) for uncracked wall sections. The secant stiffness at peak resistance was significantly lower than the effective stiffness recommended by ASCE 43-05 and ASCE 41-06 for cracked wall sections. The source of the increased flexibility has not been confirmed. Regardless of the source, the impact of a substantial reduction in effective stiffness from that traditionally assumed for analysis on the design of primary and secondary systems in safety-related nuclear structures should be carefully assessed.

3. The peak shear resistance degrades rapidly with repeated cycling at lateral displacements equal to or greater than that associated with peak shear strength. The impact of loss of strength on the seismic response and performance of safety-related nuclear structures for design basis and beyond design basis earthquake shaking should be investigated.

ACKNOWLEDGEMENT

The National Science Foundation (NEESR Program) provided the financial support for the studies described in this paper under Grant No. CMMI-0829978. The writers thank the following individuals for their contributions to the work at the University at Buffalo: Kerem Gulec (Thornton-Tomasetti, Los Angeles); Anna Birely, Laura Lowes and Joshua Pugh (University of Washington); Bozidar Stojadinovic and Catherine Whyte (University of California, Berkeley); and Abraham Lynn (California Polytechnic State University, San Luis Obispo). The authors also acknowledge the advice and assistance provided by the technical staff at the NEES Equipment Site at the University at Buffalo.

Any opinions, findings, and conclusions or recommendations expressed herein are those of the authors.

REFERENCES

American Concrete Institute Committee 318. (2011). "Building Code Requirements for Structural Concrete (ACI 318-11) and Commentary," ACI, Farmington Hills, MI.

American Society of Civil Engineers. (1998). "Seismic Analysis of Safety-Related Nuclear Structures (ASCE 4-98) and Commentary," ASCE, Reston, VA.

American Society of Civil Engineers. (2005). "Seismic Design Criteria for Structures, Systems, and Components in Nuclear Facilities (ASCE/SEI 43-05)," ASCE, Reston, VA.

American Society of Civil Engineers. (2006). "Seismic Rehabilitation of Buildings (ASCE/SEI 41-06)," ASCE, Reston, VA.

Barda, F., Hanson, J. M. and Corley, W. G. (1977). "Shear Strength of Low-rise Walls with Boundary Elements." *Reinforced Concrete Structures in Seismic Zones*, ACI, SP-53, 149-202.

Epackachi, S., Nguyen, N. H., Efe, K. G., Whittaker, A. S. and Varma, A. H. (2013). "An Experimental Study of the In-plane Shear Response of Steel Concrete Composite Walls," *Proc., 22nd International Conference on Structural Mechanics in Reactor Technology*, San Francisco, CA.

Gulec, C. K., Whittaker, A. S. and Stojadinovic, B. (2008). "Shear Strength of Squat Rectangular Reinforced Concrete Walls," *Structural Journal*, ACI, 105 (4), 488-497.

Gulec, C. K. and Whittaker, A. S. (2009). "Performance-Based Assessment and Design of Squat Reinforced Concrete Shear Walls," *Technical Report*, MCEER-09-0010, 291.

Gulec, C. K., Whittaker, A. S. and Hooper, J. D. (2010). "Fragility Functions for Low Aspect Ratio Reinforced Concrete Walls," *Engineering Structures*, 32, 2894-2901.

Gulec, C. K. and Whittaker, A. S. (2011). "Empirical Equations for Peak Shear Strength of Low Aspect Ratio Reinforced Concrete Walls," *Structural Journal*, ACI, 108 (1), 80-89.

GigaPan Systems (2013). www.gigapansystems.com.

Nikon Metrology, Inc. (2013). Krypton K600 Optical Measurement System, www.nikonmetrology.com.

Palermo, D. and Vecchio, F. J. (2002). "Behaviour and Analysis of Reinforced Concrete Walls Subjected to Reversed Cyclic Loading," ISBN 0-7727-7553-02, Publication No. 2002-01, Department of Civil Engineering, University of Toronto, Toronto, Canada.

Sozen, M. A. and Moehle, J. P. (1993). "Stiffness of Reinforced Concrete Walls Resisting In-plane Shear," *Report No. EPRI TR-102731*, Electrical Power Research Institute, Palo Alto, CA.

Whyte, C. A. and Stojadinovic, B. (2012). "Hybrid Simulation of the Seismic Response of Squat Reinforced Concrete Shear Walls", *Proc., 15th World Conference on Earthquake Engineering*, Lisbon, Portugal, paper #2551.

Wood, S. L. (1990). "Shear Strength of Low-Rise Reinforced Concrete Walls," *Structural Journal*, ACI, 87 (1), 99-107.